Equilibrium Thermodynamic Analysis of Amyotrophic Lateral Sclerosis-Associated Mutant Apo Cu,Zn Superoxide Dismutases[†,‡]

Kenrick A. Vassall,[§] Peter B. Stathopulos,[§,||] Jessica A. O. Rumfeldt,[§] James R. Lepock,[||] and Elizabeth M. Meiering*[,§]

Guelph-Waterloo Centre for Graduate Work in Chemistry and Biochemistry and Department of Chemistry and Biology, University of Waterloo, Waterloo, Ontario N2L 3G1, Canada, and Department of Medical Biophysics, Ontario Cancer Institute, University of Toronto, Toronto, Ontario M5G 2M9, Canada

Received January 17, 2006; Revised Manuscript Received April 9, 2006

ABSTRACT: The folding and thermodynamic properties of metal free (apo) superoxide dismutases (SODs) are systematically analyzed using equilibrium guanidinium chloride (GdmCl) curves and differential scanning calorimetry (DSC). Chemically and structurally diverse amyotrophic lateral sclerosis (ALS)-associated mutations (G85R, G93R, E100G, I113T) are introduced into a pseudo-wild-type background that has no free cysteines, resulting in highly reversible unfolding. Analysis of the protein concentration dependence of GdmCl curves reveals formation of a monomer intermediate in equilibrium with native dimer and unfolded monomer. Global fitting of the data enables quantitative measurement of free energy changes for both dimer dissociation and monomer intermediate stability. All the mutations decrease protein stability, mainly by destabilizing the monomer intermediate, but also by tending to weaken dimerization, even for mutations far from the dimer interface. Thus, the effects of mutations seem to propagate through the apo protein, and result in increased population of both intermediate and unfolded monomers. This may underlie increased formation of toxic aggregates by mutants in ALS. Analysis of DSC data for apo SODs is consistent with stability measurements from GdmCl curves and provides further evidence for increased aggregation by mutant proteins through increased ratios of van't Hoff to calorimetric enthalpies of unfolding.

Amyotrophic lateral sclerosis (ALS[1]) is a devastating, rapidly progressive, adult onset neurodegenerative disease. Currently, there is little effective treatment and no cure for ALS. The major known cause of the disease, representing ~1−2% of all cases, is mutations in Cu,Zn superoxide dismutase (SOD) (*1*, *2*). SOD is a homodimeric enzyme that catalyzes the dismutation of superoxide to produce hydrogen peroxide and oxygen. Each monomer consists of 153 amino acids which fold into a Greek key β-barrel and bind a structurally important Zn ion and a catalytic Cu ion (*3*, *4*) (Figure 1). Over 110 SOD mutations, distributed throughout the protein primary sequence and structure, have been associated with ALS (http://www.alsod.org) (*5*). The mutant SODs generally confer an autosomal dominant pattern of disease inheritance and are considered to have a toxic gain of function (*6*). Numerous proposals have been made

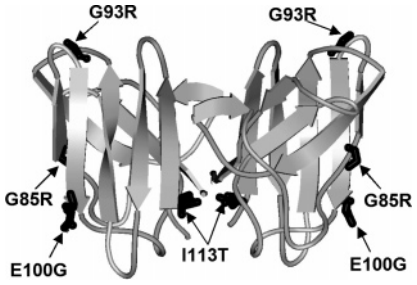

FIGURE 1: Ribbon diagram representing the crystal structure of wild-type apo SOD (pdb code 1HL4 (*43*)). Each 153 amino acid monomer of the homodimer contains 8 antiparallel β-strands which form a flattened Greek-key β-barrel. The heavy atoms of G93, G85, E100, and I113 are shown in black lines and labeled according to the corresponding ALS-associated mutations studied here (G93R, G85R, E100G, and I113T). The mutations are chemically diverse and located in different parts of the structure. E100G is located on the protein surface at the end of strand 6 and disrupts a salt bridge with K30. G85R is a located at the beginning of strand 5. G93R is located at the protein surface, in a tight turn between strands 5 and 6. These three mutations are relatively far from the dimer interface, which is formed primarily by the first and eighth β-strands as well as loops 4 and 6. I113T occurs between strands 6 and 7 in a hydrophobic patch on the monomer surface at the edge of the dimer interface. The figure was prepared using Viewer Lite Pro.

[†] This research was funded by the Neuromuscular Research Partnership, an initiative of the ALS Society of Canada, MDC, and CIHR.

[‡] In memory of James R. Lepock, our mentor, colleague, and friend.

* Corresponding author. E-mail: meiering@sciborg.uwaterloo.ca. Phone: 519-885-1211 ext 2254. Fax: 519-746-0435.

[§] University of Waterloo.

[||] University of Toronto.

[1] Abbreviations: ALS, amyotrophic lateral sclerosis; SOD, human Cu,Zn superoxide dismutase; ΔG, change in Gibbs free energy of unfolding; *m*, dependence of ΔG unfolding on denaturant concentration; GdmCl, guanidinium chloride; DSC, differential scanning calorimetry; pseudoWT (PWT), pseudo-wild-type (C6A/C111S) SOD; C_p, excess specific heat absorption; ΔC_p, change in specific heat capacity upon unfolding (kcal mol^{-1} °C^{-1}); Δh, specific enthalpy of unfolding (cal g^{-1}); ΔH, enthalpy of unfolding (kcal mol^{-1}); ΔH_{vH}, van't Hoff enthalpy of unfolding; ΔH_{cal}, calorimetric enthalpy of unfolding; β, $\Delta H_{vH}/\Delta H_{cal}$ × molecular weight of the SOD homodimer; γ, $\Delta H_{cal}/\Delta H_{vH}$; ΔS, entropy of unfolding (kcal mol^{-1} K^{-1}); *K*, equilibrium constant; T_m (t_m), temperature in K (°C) where the fraction unfolded is 0.5; t_{av}, average t_m; HEPES, hydroxyethyl piperazine *N*′-2-ethane sulfonic acid; *P*, protein concentration of dimer in M; pdb, protein data bank.

10.1021/bi0600953 CCC: $33.50
Published on Web 05/18/2006

concerning altered mutant SOD functions; however, despite extensive study, the underlying molecular mechanisms remain unclear (*7*). Recently, the hypothesis that SOD mutations cause ALS by decreasing protein stability and increasing toxic protein aggregation, as occurs in other protein misfolding diseases, has received increased attention. This hypothesis is supported by evidence from both in vivo and in vitro studies (*7*−*9*).

This paper reports characterization of the in vitro equilibrium folding mechanism and thermodynamic properties of apo SODs. Chemically and structurally diverse ALS-associated mutations (G85R, G93R, E100G, I113T, Figure 1) are introduced into a pseudo-wild-type (pseudoWT) background in which the free cysteines at positions 6 and 111 have been replaced by alanine and serine, respectively. PseudoWT has been characterized extensively in previous studies; it has very similar activity, structure, and stability to wild-type SOD, but is more amenable to in vitro analysis because the formation of aberrant disulfide bonds by the free cysteines is eliminated (*10*−*14*). Various investigations of thermal and chemical denaturation of apo wild-type and pseudoWT SOD, also incorporating ALS-associated mutations, have been reported previously (*15*−*18*); however, these did not include accurate equilibrium analysis of thermodynamic parameters. Knowledge of thermodynamic parameters is particularly important for elucidating and understanding the still elusive relationships between mutant protein properties and disease characteristics. We have conducted thermodynamic studies using guanidinium chloride (GdmCl) and differential scanning calorimetry (DSC) for pseudoWT and mutant holo SODs (*19*, *20*), and DSC for pseudoWT and G93 mutant apo SODs (*20*). Here, we extend these studies to systematically analyze highly reversible, equilibrium GdmCl denaturation curves of apo SODs, which are used to determine the thermodynamic effects of mutations on both dimer dissociation and monomer intermediate stability. The results obtained by GdmCl denaturation are consistent with results obtained by reversible thermal denaturation using DSC, which also provides evidence for increased aggregation by mutant proteins. These studies give important information on the relative stability and equilibrium populations of different states of this dimeric protein, and give insights into possible mechanisms of SOD aggregation in ALS.

MATERIALS AND METHODS

Preparation and Purification of Recombinant SOD. ALS-associated mutations (G85R, G93R, E100G, I113T) were introduced into the pseudoWT SOD gene using the plasmid vector pPHSOD1ASLacI^q, and expressed as previously described (*14*, *21*). The produced protein lacked the native N-terminal acetylation; this is unlikely to have a significant effect on folding owing to the unstructured nature of the SOD N-terminus and its location on the surface of the molecule away from the dimer interface. This is further supported by close similarities in the stability of the acetylated and the nonacetylated SOD (*16*, *22*). The proteins were purified using a modification of the procedure of Getzoff et al. (*21*) in which the diethylaminoethyl column was replaced by a Poros HP2 hydrophobic interaction column. Metals were removed to make the apo protein by dialyzing against ethylenediaminetetraacetic acid (*23*). Removal of metals was confirmed by the presence of a single peak in the DSC unfolding thermograms and by inductively coupled plasma atomic emission spectroscopy (Solutions Analytical Laboratory, University of Waterloo, Waterloo, Ontario, Canada). Protein concentrations were determined by the Lowry method (*24*).

Differential Scanning Calorimetry. The methodology for DSC measurements was as described (*20*). Measurements were made using a MicroCal LLC VP-DSC (MicroCal Inc., Northampton, MA). All samples contained 0.1 to ~2 mg mL^{-1} protein in 20 mM hydroxyethyl piperazine *N*′-2-ethane sulfonic acid (HEPES), pH 7.8. The scan rate was 1 °C min^{-1}.

Equilibrium Chemical Denaturation and Renaturation Curves. Equilibrium denaturation curves were obtained for apo pseudoWT and mutants by diluting 10× concentrated stock protein into solutions containing HEPES and different concentrations of the denaturant GdmCl. The final concentration of HEPES was 20 mM, pH 7.8. For curves obtained in sodium sulfate, this was added to the mixture to a final concentration of 0.75 M. Samples were equilibrated at 25 °C by incubating in a temperature-controlled water bath. Renaturation curves were acquired using the same methodology with the exception that the stock protein solution was first denatured in 4 M GdmCl before dilution into the appropriate solutions. Circular dichroism (CD) measurements at 216 and 231 nm were carried out using a J715 CD spectropolarimeter (Jasco) equipped with a Peltier temperature-controlled cell holder. Steady state fluorescence measurements were made using a Fluorolog3-22 (Instruments SA, Edison, NJ) with a thermostated water-jacketed cuvette holder, with excitation and emission wavelengths of 282 nm and 360 nm, respectively.

DSC Data Analysis. DSC data were fit as described previously (*20*, *25*). Buffer/buffer scans were subtracted from protein/buffer scans, which were then normalized for protein concentration, and fit to a dimer 2-state model: $N_2 \leftrightarrows 2U$, where N_2 is the native dimer and 2U are unfolded monomers, according to the equation

$$C_p^{tot}(T) = \frac{\beta \Delta h^2(T)}{RT^2} \frac{f_u(1-f_u)}{2-f_u} + (1-f_u)(A+BT) + f_u(C+DT) \quad (1)$$

where $C_p^{tot}(T)$ is the total specific heat absorption at T (in K), f_u is the fraction of unfolded protein at T, $\Delta h(T)$ is the specific enthalpy of unfolding at T, A and B are the intercept and slope of the native baseline, respectively, while C is the intercept of the unfolded baseline and D is its slope, and β is a temperature-independent constant equal to the molecular weight of the dimer multiplied by the ratio of van't Hoff to calorimetric enthalpies of unfolding ($\Delta H_{vH}/\Delta H_{cal}$). A ratio >1 indicates that the cooperative unfolding unit is larger than the dimer (e.g. oligomer and/or aggregate), while a ratio <1 indicates that unfolding occurs via the formation of one or more intermediates (*20*, *26*). For comparison, data were also analyzed using a unimolecular monomer 2-state model ($N \leftrightarrows U$) according to the following equation:

$$C_p^{ex}(T) = \frac{\gamma \Delta H^2(T) f_u(1-f_u)}{RT^2} \quad (2)$$

where $C_p^{ex}(T)$ and $\Delta H(T)$ are the excess specific heat absorption and the enthalpy of unfolding, respectively, at T and γ is ($\Delta H_{vH}/\Delta H_{cal}$). All data analysis was performed using Origin 5.0 SR2 (Microcal Inc.).

ΔH_{vH}, which had far less variability than ΔH_{cal} and corresponds to a molecularity of 2 (as expected for a dimer unfolding transition (*20*)), determined from a plot of ln P versus $1/T_m$, was used to calculate the Gibbs free energy of unfolding (ΔG) according to

$$\Delta G(T) = \Delta H_{vH}(T) - T\Delta S(T) \quad (3)$$

$$\Delta H_{vH}(T) = \Delta H_{vH}(T_m) + \Delta C_p(T - T_m) \quad (4)$$

$$\Delta S(T) = \Delta S(T_m) + \Delta C_p \ln \frac{T}{T_m} \quad (5)$$

and

$$\Delta S(T_m) = \frac{\Delta H(T_m) - \Delta G(T_m)}{T_m} \quad (6)$$

where $\Delta S(T)$ is the entropy of unfolding at T, T_m is the temperature at which the fraction of unfolded molecules $f_u = 0.5$, and ΔC_p is the change in heat capacity. A temperature-independent ΔC_p of 3.30 kcal mol^{-1} °C^{-1} was used to calculate ΔG; this value was obtained from a previous calorimetric study on apo pseudoWT and mutants under conditions identical to those of this study (*20*).

GdmCl Curve Analysis. Chemical denaturation data were fit to equations for a dimer 2-state model and 3-state models with monomer or dimer intermediate (*19*, *27*).

Equations. The optical signal of each structural probe Y_o is proportional to the intrinsic signal of each species i present at equilibrium such that

$$Y_o = \sum X_i Y_i \quad (7)$$

where X_i is the mole fraction of each species and Y_i is its spectroscopic signal. The signal of each species varies linearly with [GdmCl] such that

$$Y_i = Y_{H_2O,i} + s_i[\text{GdmCl}] \quad (8)$$

where $Y_{H_2O,i}$ is the signal of a particular species i at 0 M GdmCl and s_i describes the dependence of the signal on [GdmCl]. From the mole fractions of each species i, the equilibrium constant of unfolding, K, and hence ΔG can be determined at each [GdmCl]. The ΔG at 0 M GdmCl can then be determined based on extrapolation, assuming a linear dependence of ΔG with [GdmCl] such that

$$\Delta G = -RT \ln K = \Delta G_{H_2O} + m[\text{GdmCl}] \quad (9)$$

where ΔG_{H_2O} is the Gibbs free energy at 0 M GdmCl, m describes the magnitude of the dependence of ΔG on [GdmCl], R is the universal gas constant, and T is the absolute temperature in K.

In a dimer 2-state model, only the native (N_2) and the unfolded (U) states of the protein are populated at equilibrium ($N_2 \leftrightarrows 2U$). The equilibrium constant K for this process is defined as

$$K = \frac{[U]^2}{[N_2]} \quad (10)$$

Equation 7 can be expressed with respect to equilibrium constant K and total protein concentration P (expressed as concentration of dimer in M):

$$Y_o = Y_n\left(1 - \left(\frac{\sqrt{K^2 + 16KP} - K}{8P}\right)\right) + Y_u\left(\frac{\sqrt{K^2 + 16KP} - K}{8P}\right) \quad (11)$$

where Y_n and Y_u are the spectroscopic signals for the native (N_2) and the unfolded (U) states, respectively.

In a 3-state model, either a monomer intermediate (I) or a dimer intermediate (I_2) is also populated at equilibrium. For the 3-state monomer intermediate model ($N_2 \leftrightarrows 2I \leftrightarrows 2U$), the two equilibrium constants K_1 and K_2 that define each unfolding step are given by

$$K_1 = \frac{[I]^2}{[N_2]} \quad (12)$$

and

$$K_2 = \frac{[U]}{[I]} \quad (13)$$

Equation 7 is defined in terms of K_1, K_2, and P such that the final equation used for fitting is

$$Y_o = \left(Y_n + (Y_j - Y_n + K_2(Y_u - Y_n))\left(\frac{\sqrt{K_1^2(1 + K_2)^2 + 16K_1P} - K_1(1 + K_2)}{8P}\right)\right) \quad (14)$$

where the subscripts n, j, and u indicate native dimer, intermediate, and unfolded monomer, respectively.

In the 3-state model with dimer intermediate ($N_2 \leftrightarrows I_2 \leftrightarrows 2U$), the equilibrium constants K_1 and K_2 are given by

$$K_1 = \frac{[I_2]}{[N_2]} \quad (15)$$

and

$$K_2 = \frac{[U]^2}{[I_2]} \quad (16)$$

Data were fit to

$$Y_o = \left(Y_u + (Y_n - Y_u + K_1(Y_j - Y_u)) \left(1 - \left(\frac{\sqrt{(K_1K_2)^2 + 16(1+K_1)(K_1K_2)P} - K_1K_2}{8P(1+K_1)} \right) \right) \right) \frac{1}{1+K_1} \quad (17)$$

Data Fitting. Fits to individual GdmCl curves were performed using MATLAB software, version 7.0.4 (The MathWorks Inc.), while global fits for multiple curves were performed with Origin 5.0 SR2 (Microcal Inc.). Due to the many parameters inherent to these models, the fitting programs could not provide an accurate fit if all were allowed to vary. The following steps were taken to address this. The slope and intercept of the native and unfolded baselines were first fit using linear regression analysis and fixed in subsequent fitting. The native baseline was most pronounced and least scattered for the highest concentration curves. Hence, the slope and intercept for the native baseline of the highest concentration curves of each dataset were used for lower protein concentrations with appropriate scaling. Due to the increased scatter of CD data, the native baseline used for the fits was an average slope and intercept of all 30 μM curves.

Despite the above simplifications, fits of individual datasets to 3-state models was precluded due to large errors reported by the fitting programs. However, multiple datasets could be accurately fit simultaneously with ΔG and m values as globally shared parameters. CD and fluorescence datasets were considered separately for the global fits. In all 3-state monomer intermediate fits, the slope of the intermediate was set to 0. For fluorescence data acquired in sodium sulfate, the signal of the intermediate was set to a value of 30% of the total amplitude (unfolded signal − native signal) of the transition. This value of 30% was determined by globally fitting the 1, 5, 10, and 30 μM fluorescence datasets of pseudoWT in 0.75 M Na_2SO_4, and systematically changing the magnitude of the intermediate signal from 10% to 80% of the total amplitude of the transition. The value of 30% corresponded to the lowest χ^2 value for fitting. Due to the lower population of intermediate and the less pronounced native baselines of denaturation curves acquired in the absence of sodium sulfate, determination of the intermediate fluorescence value was less accurate. This was compounded by nonlinear native baseline effects resulting from GdmCl (see Results). Hence, the better defined intermediate fluorescence value of 30% obtained from data in sodium sulfate was also used for data without sodium sulfate. For CD data, the intermediate is ill-defined likely due to the increased scatter of the data and the higher protein concentrations that were required (owing to the lower sensitivity of the probe). Varying the intermediate value from 20% to 80% produced little variation in m and ΔG (~10%). The value of 30% was therefore used for all 3-state monomer intermediate fits. It should be noted that the signal for the intermediate will not in general be the same when measured by different optical probes; however, the approach taken above is experimentally reasonable and has little effect on the fitted values.

For the determination of ΔGs (Table 1) for all probes using a 3-state monomer intermediate model, data obtained in 0.75 M Na_2SO_4 were fit to a fixed m_1 (the dependence of the free energy of dimer dissociation, ΔG_1, on denaturant concentration) value of 1.4 kcal (mol dimer)$^{-1}$ M^{-1} and a fixed m_2 (the dependence of the free energy of intermediate unfolding, ΔG_2, on denaturant concentration) value of 3.5 kcal (mol monomer)$^{-1}$ M^{-1}. These m values were determined by globally fitting each mutant and pseudoWT datasets from all 3 probes (fluorescence, CD 216 nm and CD 231 nm) and averaging the resulting m values. For the pseudoWT datasets without sodium sulfate, the m values were best defined by the fluorescence results, thus the values of m_1 = 2.7 kcal (mol dimer)$^{-1}$ M^{-1} and m_2 = 2.6 kcal (mol monomer)$^{-1}$ M^{-1} obtained from the fluorescence global fit were also used for fitting CD datasets. Regardless of the intermediate and m values used in fitting, the 3-state model with dimer intermediate did not account well for the data across all three probes in this study.

RESULTS

Denaturation of Apo PseudoWT and Mutant SODs Is Highly Reversible. Chemical denaturation of pseudoWT and mutant apo SODs by GdmCl, monitored by fluorescence and circular dichroism (CD) at 216 and 231 nm, is highly reversible. This is evidenced by the congruence of denaturation and renaturation curves, with equilibrium being reached within ~48 h of incubation for denaturation curves and ~72 h for renaturation curves (Figures 2 and 3). Chemical denaturation of holo SODs has been found previously to also be highly reversible under these conditions; however the holo proteins take much longer (many days) to reach equilibrium (*19*). The shape of the apo SOD curves is similar to curves obtained for holo, but the former are shifted by >2 M to lower GdmCl concentrations. There is a nonlinear decrease in fluorescence at low denaturant concentrations (Figure 3), which has been shown not to be associated with a significant cooperative structural transition for holo (*19*). As expected for a dimeric protein, the curves depend significantly on protein concentration, with transition midpoints shifting to higher GdmCl concentration with increasing protein concentration (Figures 2, 3, and 5).

Thermal denaturation of apo SODs is also highly reversible, as determined by calculating the areas of unfolding endotherms from successive DSC heating scans. Reversibility was highest (>95%) when scans were conducted just to the end of the unfolding endotherms (data not shown) as has been observed also for other mutants (*20*). The mutants showed greater reversibility than pseudoWT, probably because they were scanned to lower temperatures owing to their decreased melting points (*20*).

Sodium Sulfate Markedly Stabilizes PseudoWT and Mutant Apo SODs. Owing to nonlinear effects of GdmCl on fluorescence at low GdmCl (see above) and decreased transition midpoints, GdmCl curves for apo mutants have ill-defined native baselines (data not shown). In order to facilitate chemical denaturation analysis of mutants, GdmCl curves were also measured with the addition of the stabilizing agent, sodium sulfate. The addition of 0.75 M sodium sulfate increases the midpoint of chemical denaturation by ~1.9 M GdmCl (Figures 2 and 3). This results in a much better

Table 1: Thermodynamic Parameters from GdmCl Curves of PseudoWT and Mutant Apo SODs

				dimer 2-state model		dimer 3-state with monomer intermediate[a]		
protein	$[Na_2SO_4]$ (M)	[protein] (μM)	probe	m_{total}[c] (kcal (mol dimer)$^{-1}$ M^{-1})	ΔG_{total}[c] ($N_2 \leftrightarrows 2U$) (kcal (mol dimer)$^{-1}$)	ΔG_1[c] ($N_2 \leftrightarrows 2I$) (kcal (mol dimer)$^{-1}$)	ΔG_2[c] ($I \leftrightarrows U$) (kcal (mol monomer)$^{-1}$)	ΔG_{total}[d,e] ($N_2 \leftrightarrows 2I \leftrightarrows 2U$) (kcal (mol dimer)$^{-1}$)
PWT	0	0.2	Fl	5.5 ± 0.8	13.4 ± 0.7			
PWT	0	1	Fl	7.4 ± 0.5	15.6 ± 0.5			
PWT	0	5	Fl	7.7 ± 0.6	15.9 ± 0.7			
PWT	0	10	Fl	8.5 ± 0.7	16.7 ± 0.8			
PWT	0	0.2, 1, 5, 10[b]	Fl	7.3 ± 0.2	15.3 ± 0.2	12.4 ± 0.7	1.8 ± 0.4	16.0 ± 0.9
PWT	0	5	CD_{216}	6.6 ± 0.9	15 ± 1			
PWT	0	10	CD_{216}	8.4 ± 0.9	17 ± 1			
PWT	0	5, 10[b]	CD_{216}	7.7 ± 0.7	15.8 ± 0.8	12.7 ± 0.5	1.7 ± 0.2	16.1 ± 0.6
PWT	0	10	CD_{231}	9 ± 1	17 ± 2	13.3 ± 0.6	1.3 ± 0.3	15.9 ± 0.7
PWT	0.75	1	Fl	4.4 ± 0.5	21 ± 1			
PWT	0.75	5	Fl	6.9 ± 0.4	28 ± 1			
PWT	0.75	10	Fl	6.4 ± 0.5	26 ± 1			
PWT	0.75	30	Fl	6.9 ± 0.8	28 ± 3			
PWT	0.75	1, 5, 10, 30[b]	Fl	6.5 ± 0.2	26.7 ± 0.6	12.0 ± 0.1	10.33 ± 0.04	32.7 ± 0.1
PWT	0.75	5	CD_{216}	6.1 ± 0.7	25 ± 2			
PWT	0.75	10	CD_{216}	7.8 ± 0.8	29 ± 2			
PWT	0.75	30	CD_{216}	6.3 ± 0.9	26 ± 3			
PWT	0.75	5, 10, 30[b]	CD_{216}	6.3 ± 0.3	26 ± 1	11.9 ± 0.1	10.5 ± 0.1	32.9 ± 0.2
PWT	0.75	5	CD_{231}	7 ± 1	30 ± 3			
PWT	0.75	10	CD_{231}	8 ± 1	30 ± 3			
PWT	0.75	30	CD_{231}	7.8 ± 0.5	31 ± 2			
PWT	0.75	5, 10, 30[b]	CD_{231}	6.6 ± 0.4	27 ± 1	12.3 ± 0.3	10.2 ± 0.1	32.7 ± 0.3
G85R	0.75	1	Fl	5.3 ± 0.5	21 ± 1			
G85R	0.75	5	Fl	7.5 ± 0.5	26 ± 1			
G85R	0.75	30	Fl	7.3 ± 0.8	26 ± 2			
G85R	0.75	1, 5, 30[b]	Fl	6.6 ± 0.2	23.8 ± 0.4	11.7 ± 0.1	8.4 ± 0.1	28.5 ± 0.2
G85R	0.75	10	CD_{216}	7.2 ± 0.6	26 ± 2			
G85R	0.75	30	CD_{216}	6.0 ± 0.6	22 ± 2			
G85R	0.75	10, 30[b]	CD_{216}	7.0 ± 0.2	25.0 ± 0.5	11.5 ± 0.2	8.6 ± 0.1	28.7 ± 0.2
G85R	0.75	30	CD_{231}	7.6 ± 0.6	27 ± 2	11.7 ± 0.3	8.6 ± 0.2	28.9 ± 0.4
E100G	0.75	1	Fl	5.2 ± 0.6	20 ± 1			
E100G	0.75	3	Fl	5.8 ± 0.8	22 ± 2			
E100G	0.75	10	Fl	6.5 ± 0.5	23 ± 1			
E100G	0.75	30	Fl	7.4 ± 0.5	26 ± 1			
E100G	0.75	1, 3, 10, 30[b]	Fl	6.9 ± 0.2	24.4 ± 0.4	11.3 ± 0.1	8.47 ± 0.05	28.2 ± 0.1
E100G	0.75	5	CD_{216}	6.2 ± 0.9	22 ± 2			
E100G	0.75	10	CD_{216}	7.7 ± 0.8	26 ± 1			
E100G	0.75	30	CD_{216}	6.5 ± 0.8	23 ± 2			
E100G	0.75	5, 10, 30[b]	CD_{216}	6.8 ± 0.2	23.9 ± 0.5	11.4 ± 0.2	8.3 ± 0.1	28.0 ± 0.2
E100G	0.75	5	CD_{231}	5 ± 1	20 ± 3			
E100G	0.75	10	CD_{231}	7.8 ± 0.8	27 ± 2			
E100G	0.75	30	CD_{231}	7.3 ± 0.6	25 ± 2			
E100G	0.75	5, 10, 30[b]	CD_{231}	6.8 ± 0.3	24.2 ± 0.7	11.0 ± 0.2	8.6 ± 0.1	28.2 ± 0.2
G93R	0.75	1	Fl	5.5 ± 0.4	21 ± 1			
G93R	0.75	3	Fl	7.5 ± 0.6	25 ± 1			
G93R	0.75	10	Fl	7.5 ± 0.4	25 ± 1			
G93R	0.75	1, 3, 10[b]	Fl	7.9 ± 0.2	26.1 ± 0.5	11.7 ± 0.1	7.8 ± 0.1	27.3 ± 0.2
G93R	0.75	3	CD_{216}	7 ± 1	23 ± 3			
G93R	0.75	10	CD_{216}	9.0 ± 0.9	29 ± 2			
G93R	0.75	3, 10[b]	CD_{216}	7.5 ± 0.3	25.2 ± 0.8	12.0 ± 0.5	7.7 ± 0.2	27.4 ± 0.6
G93R	0.75	3	CD_{231}	9 ± 2	28 ± 5			
G93R	0.75	10	CD_{231}	6.3 ± 0.7	22 ± 1			
G93R	0.75	3, 10[b]	CD_{231}	9.4 ± 0.3	30.2 ± 0.7	11.8 ± 0.5	7.8 ± 0.3	27.4 ± 0.7
I113T	0.75	1	Fl	4.4 ± 0.3	17.1 ± 0.7			
I113T	0.75	5	Fl	5.8 ± 0.2	19.8 ± 0.5			
I113T	0.75	30	Fl	7.8 ± 0.8	24 ± 2			
I113T	0.75	1, 5, 30[b]	Fl	7.1 ± 0.3	22.7 ± 0.6	10.6 ± 0.1	7.56 ± 0.04	25.7 ± 0.1
I113T	0.75	5	CD_{216}	5.9 ± 0.7	20 ± 2			
I113T	0.75	30	CD_{216}	7.2 ± 0.6	23 ± 2			
I113T	0.75	5, 30[b]	CD_{216}	6.8 ± 0.3	22.3 ± 0.6	10.8 ± 0.2	7.6 ± 0.1	26.0 ± 0.2
I113T	0.75	5	CD_{231}	6 ± 1	21 ± 3			
I113T	0.75	30	CD_{231}	7.1 ± 0.3	23.1 ± 0.8			
I113T	0.75	5, 30[b]	CD_{231}	7.4 ± 0.3	23.8 ± 0.8	10.9 ± 0.3	7.7 ± 0.1	26.3 ± 0.3

[a] For data with 0 M Na_2SO_4, m_1 and m_2 were fixed to 2.7 kcal (mol dimer)$^{-1}$ M^{-1} and 2.6 kcal (mol monomer)$^{-1}$ M^{-1}, respectively, while with 0.75 M Na_2SO_4, m_1 and m_2 were fixed to 1.4 kcal (mol dimer)$^{-1}$ M^{-1} and 3.5 kcal (mol monomer)$^{-1}$ M^{-1}, respectively. [b] Data were fit globally with *m*s and ΔGs as shared parameters. [c] Errors are from the fitting program. [d] $\Delta G_{total} = \Delta G_1 + 2\Delta G_2$. [e] Errors were propagated according to standard procedures (*67*).

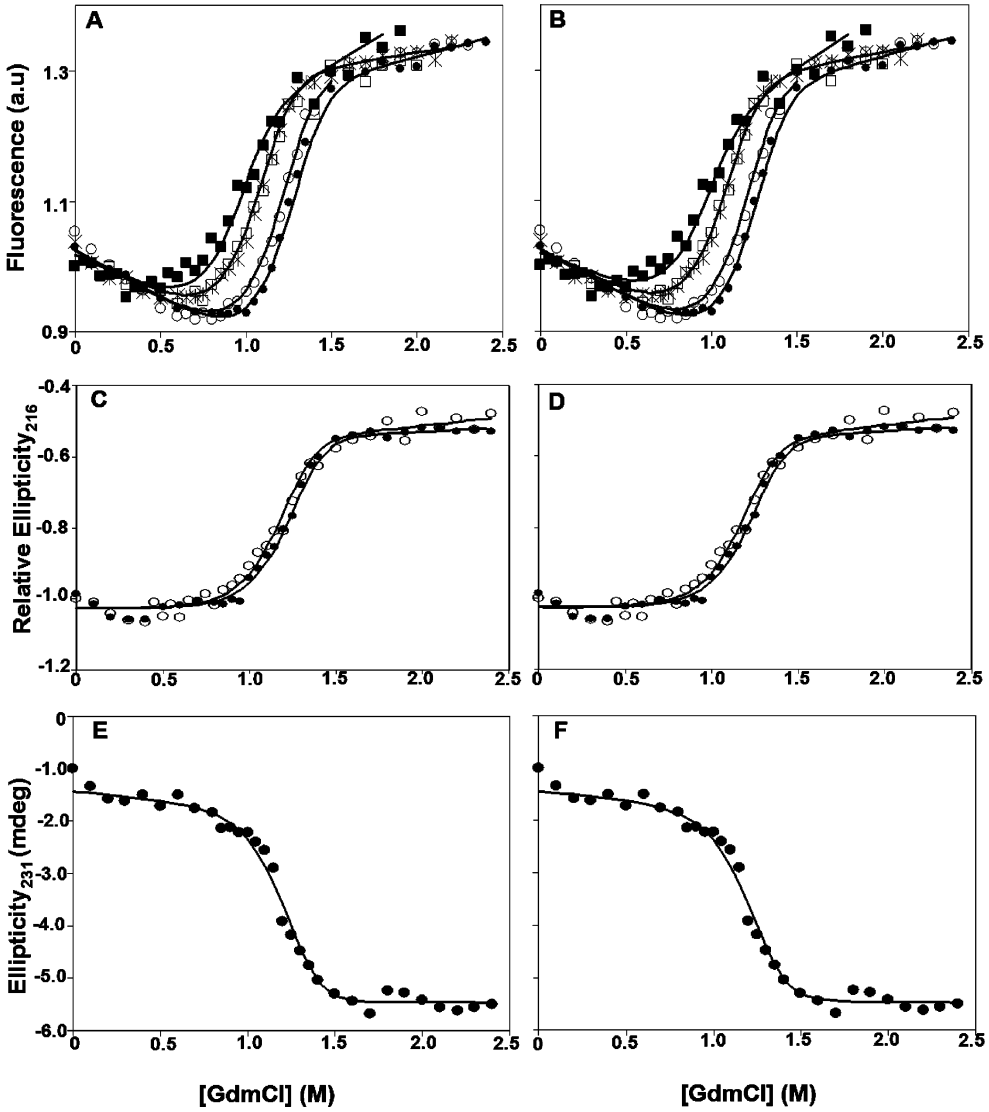

FIGURE 2: Protein concentration dependence of equilibrium denaturation curves for apo pseudoWT, in 20 mM HEPES, pH 7.8, 25 °C. Protein concentrations are 0.2 μM (■), 1 μM (*), 5 μM (○), and 10 μM (●). A 1 μM renaturation curve (□) is also shown to illustrate the reversibility of unfolding. Data are normalized and offset for differences in protein concentration to facilitate comparison. Curves were monitored by (A, B) fluorescence, (C, D) CD at 216 nm, and (E, F) CD at 231 nm. The lines correspond to fits (Table 1) for each optical probe to a dimer 2-state model (A, C, E) and a 3-state model with monomer intermediate (B, D, F). Multiple datasets for each probe were fit globally.

defined native baseline, enabling a more accurate thermodynamic analysis (see below). The CD spectra of both native and unfolded apo SOD are very similar with and without sodium sulfate (data not shown). This indicates that sodium sulfate does not induce a major structural change in these states.

GdmCl Curve Fitting to 2-State and 3-State Models. Apo pseudoWT equilibrium chemical denaturation curves monitored by fluorescence as well as CD at 216 and 231 nm, both with and without Na_2SO_4, were initially fit to a dimer 2-state model for a transition between folded dimer (N_2) and unfolded monomer (U): $N_2 \leftrightarrows 2U$ (Figures 2, and 3 and Table 1). Curves were fit (see Materials and Methods) individually as well as globally with ΔG_{total} (Gibbs free energy of unfolding) and m_{total} (dependence of ΔG_{total} on denaturant concentration) as shared parameters (Table 1). Although the global 2-state fits for apo pseudoWT with 0 M Na_2SO_4 pass through the data points fairly well, there is a systematic deviation for the lowest protein concentrations and global fit m_{total} and ΔG_{total} values are somewhat lower than expected (Figure 2, Table 1, and below). In addition, inspection of ΔG_{total} and m_{total} values for fits to individual curves reveals systematic increases with increasing protein concentration (Table 1). Low and changing m and ΔG values are often indicative of population of an intermediate (*28*). The changes in values are more pronounced at lower protein concentrations and become smaller at higher protein concentrations. Similar results were also obtained for holo SODs, where unfolding is close to 2-state at high protein concentration but a folded monomer intermediate becomes significantly populated at low protein concentration (*19*). Deviation from a 2-state global fit at low protein concentration is more apparent for data acquired in 0.75 M Na_2SO_4 (Figure 3, Table 1).

Due to the deviations for the 2-state fits, the data were also fit to 3-state models with monomer (I) or dimer intermediate (I_2). The data without and with sodium sulfate are not well fit by the dimer intermediate model ($N_2 \leftrightarrows I_2$

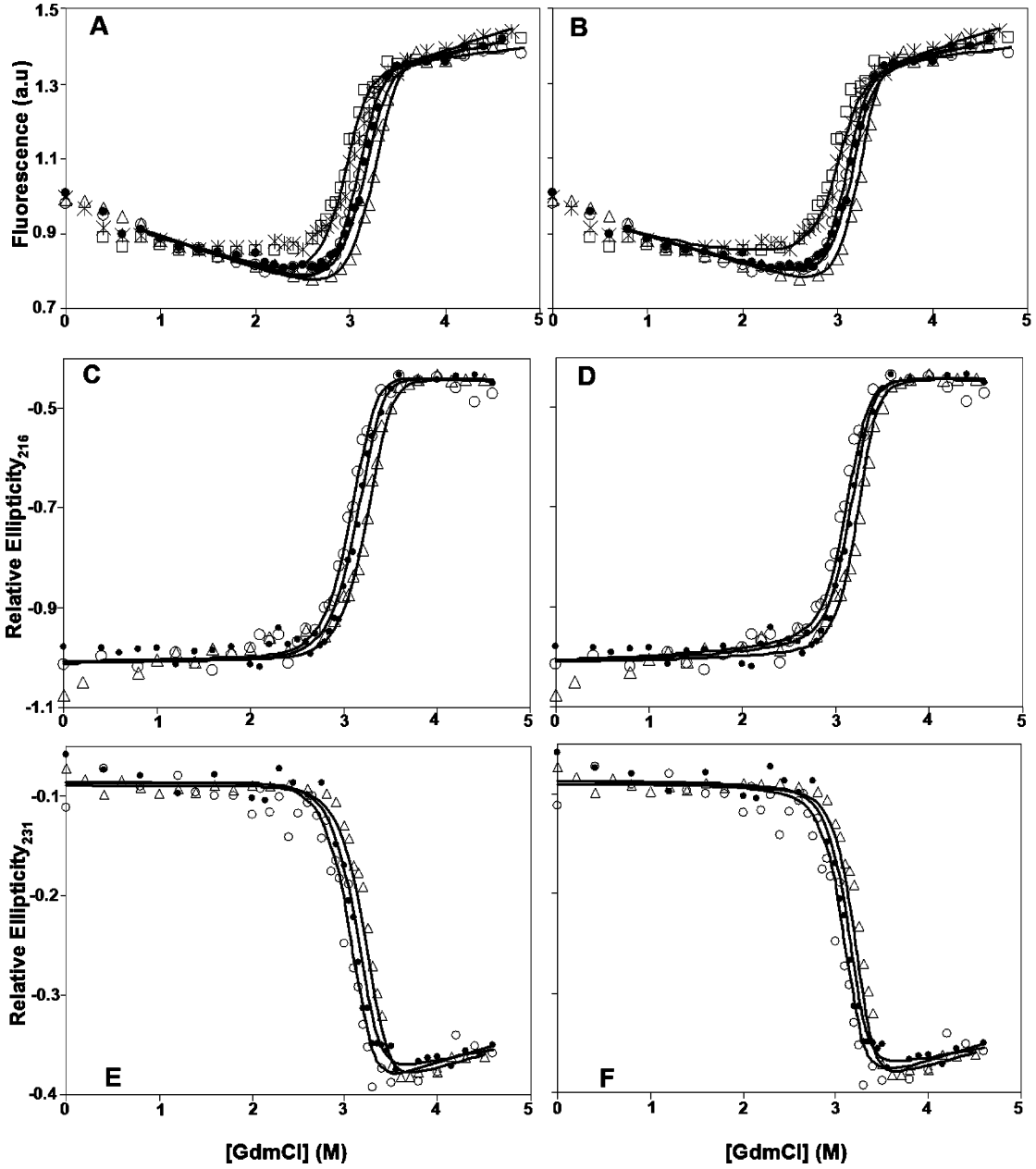

FIGURE 3: Protein concentration dependence of equilibrium denaturation curves of apo pseudoWT in 0.75 M sodium sulfate, 20 mM HEPES, pH 7.8, 25 °C. Protein concentrations are 1 μM (*), 5 μM (○), 10 μM (●), and 30 μM (△). A 1 μM renaturation curve (□) is also shown. Data are normalized for protein concentration and offset to facilitate comparison. Lines corresponding to global dimer 2-state (A, C, E) and 3-state monomer intermediate (B, D, F) fits for curves monitored by (A, B) fluorescence, (C, D) CD at 216 nm, and (E, F) CD at 231 nm are also shown. Fluorescence data below 0.8 M GdmCl were not included in the fit due to nonlinear optical effects at low denaturant (see Results). The fits demonstrate that data at high protein concentrations are well accounted for by the 2-state fits. At lower protein concentrations a monomer intermediate becomes increasingly populated leading to deviations from 2-state fits. This is most apparent for the 1 μM curve. Parameters for fits to a global 3-state model with a monomer intermediate as well as to a dimer 2-state model are given in Table 1.

$\leftrightarrows$ 2U), but are well fit by the monomer intermediate model ($N_2 \leftrightarrows 2I \leftrightarrows 2U$) over the full protein concentration range (Figures 2 and 3), enabling determination of both ΔG_1 (Gibbs free energy of dimer dissociation) and ΔG_2 (Gibbs free energy of monomer intermediate unfolding) (Table 1). The resulting fitted values are consistent across all structural probes (Table 1). The ΔG_{total} ($\Delta G_{total} = \Delta G_1 + 2\Delta G_2$) in the absence of sodium sulfate is 16.0 kcal (mol dimer)$^{-1}$ (averaged across all three probes). This value is very similar to the value determined by DSC (*20*) (see below).

Fits of the data obtained with sodium sulfate give a ΔG_{total} of 32.8 kcal (mol dimer)$^{-1}$, indicating a significant stabilizing effect of sodium sulfate, comparable to effects observed for other proteins (*29*, *30*); this stabilization may well be biologically relevant (see Discussion). Interestingly, the values of ΔG_1 without and with sodium sulfate are quite similar at 12.1 and 12.8 kcal (mol dimer)$^{-1}$, respectively. In contrast, ΔG_2 increases from 1.6 kcal (mol monomer)$^{-1}$ to 10.3 kcal (mol monomer)$^{-1}$. Thus, the overall stabilizing effect of sodium sulfate is dominated by the effect on the monomer intermediate. As a consequence, there is a significant increase in the population of the monomer intermediate in sodium sulfate (Figure 4). The values of m_{total} ($m_{total} = m_1 + 2m_2$; where m_1 and m_2 are the denaturant dependence

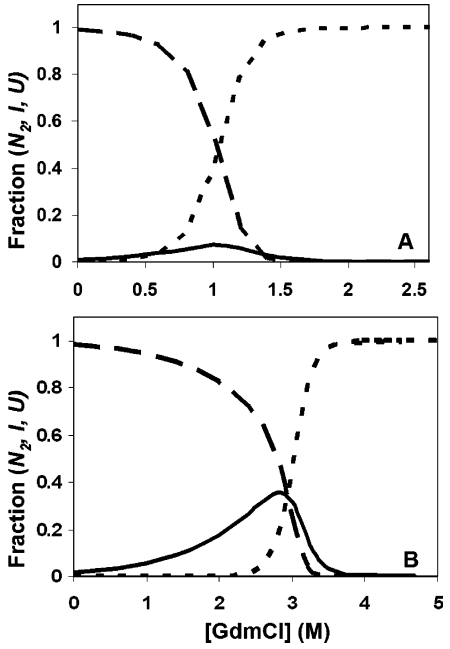

FIGURE 4: Fractions of the native dimer (− − −), monomer intermediate (—), and denatured monomer (- - -) as a function of GdmCl concentration for 1 μM apo pseudoWT. Comparison of the fractions of these various protein conformations in (A) 0 M sodium sulfate and (B) 0.75 M sodium sulfate demonstrate that the monomer intermediate is much more populated in sodium sulfate as evidenced by the maximal fraction of intermediate increasing from 0.07 without sodium sulfate to 0.35 in sodium sulfate.

of ΔG_1 and ΔG_2, respectively) are similar without and with sodium sulfate, 7.9 kcal (mol dimer)$^{-1}$ M^{-1} and 8.4 kcal (mol dimer)$^{-1}$ M^{-1}, respectively. These values are very close to the values calculated using empirical formulas and measured for holo SODs (*19*). Despite these similarities, m_1 decreases from 2.7 to 1.4 kcal (mol dimer)$^{-1}$ M^{-1} in sodium sulfate, while m_2 increases from 2.6 to 3.5 kcal (mol monomer)$^{-1}$ M^{-1}, suggesting that the intermediate becomes more compact in sodium sulfate (see Discussion). Due to relatively high uncertainties in fitting data without sodium sulfate (see Materials and Methods), it is unclear whether this compaction results in altered spectroscopic properties of the intermediate.

GdmCl Denaturation of Mutant Apo SODs. The effects of mutations on folding mechanism and stability were investigated by obtaining GdmCl denaturation curves monitored by fluorescence and CD as a function of protein concentration for apo G85R, E100G, G93R, and I113T (Figure 5, Table 1). As for pseudoWT, the mutant data are best fit by the monomer intermediate model. The changes in total Gibbs free energy of unfolding from native dimer to unfolded monomers, $\Delta\Delta G_{\text{total}}$ ($\Delta\Delta G_{\text{total}} = \Delta G_{\text{total}}^{\text{mutant}} - \Delta G_{\text{total}}^{\text{pseudoWT}}$), show that all the mutants are destabilized relative to the wild-type protein (Table 3), as expected based on the decreased midpoints of unfolding (Figures 3 and 5). The order of stability, from most stable to least stable, is G85R > E100G > G93R > I113T. Both dimer dissociation (ΔG_1) and monomer stability (ΔG_2) are negatively affected by the mutations, with the destabilization of the monomer being the greater contributor to the decease in overall stability (Table 3). Despite the smaller impact on ΔG_1, these differences in stability significantly increase the relative population of intermediate (Figure 6). For example, for G93R, although ΔG_1 is decreased just 0.3 kcal (mol dimer)$^{-1}$, the ratio of monomer intermediate concentration of mutant relative to pseudoWT is ~1.3 (i.e. 30% increase in intermediate concentration). G85R, E100G, and I113T have larger effects on ΔG_1 and the ratio of intermediate concentration is increased to ~ 1.5, 2, and 3, respectively. The mutations cause even larger effects on the populations of unfolded monomers. For the G93R mutation the ratio of concentration of unfolded monomers of mutant relative to pseudoWT is 85 (i.e. the concentration of unfolded monomers is increased 85-fold, or 8500%), while the ratios for G85R, E100G, and I113T are ~30, 40, and 280, respectively.

Differential Scanning Calorimetry of Mutant Apo SODs. Mutant stability was also assessed by differential scanning calorimetry (Table 2). Good quality data were obtained without sodium sulfate, with melting temperatures ranging from ~45 to 62 °C. Thermal denaturation of pseudoWT and mutants is well fit using a dimer 2-state unfolding scheme between native dimer (N_2) and unfolded monomers (2U), allowing both ΔH_{vH} and ΔH_{cal} to vary (Figure 7). Data were also fit to a 2-state monomer unfolding model (N ⇆ U), which clearly accounted less well for the data (data not shown). For dimer 2-state fitting, the $\Delta H_{\text{vH}}/\Delta H_{\text{cal}}$ ratio is ~1 for pseudoWT, but is significantly larger than 1 for the mutants. This has also been observed for other ALS-associated mutant apo SODs (*20*) and appears to be a common characteristic of these mutants. $\Delta H_{\text{vH}}/\Delta H_{\text{cal}} > 1$ is evidence for increased formation of aggregates by the mutants (*20*, *25*, *31*). Note that formation of monomer or unfolding via any intermediate would cause $\Delta H_{\text{vH}}/\Delta H_{\text{cal}} < 1$ (*26*), which is not apparent in the DSC data. The evidence for aggregation of mutant SODs during thermal unfolding is in contrast to the GdmCl data where there is no indication of protein aggregation; however, it should be noted that GdmCl and sodium sulfate may inhibit aggregation.

The relative stability of the mutants in DSC experiments is the same as measured by chemical denaturation (Table 3). The magnitudes of the destabilization ($\Delta\Delta G_{\text{total}}$) of the mutants are slightly smaller, however, when measured by DSC (Table 3); this is likely due to the effects of sodium sulfate (see Discussion). Changes in ΔH and ΔS due to the mutations relative to pseudoWT are reported in Table 2 as $\Delta\Delta H$ and $\Delta\Delta S$. For G85R, E100G, and G93R, destabilization is entropically driven (i.e. positive $\Delta\Delta S$), while destabilization of I113T is enthalpically driven (i.e. negative $\Delta\Delta H$). It is difficult to rationalize the mechanism of destabilization in terms of enthalpy and entropy for each mutation since both changes in noncovalent interactions within the polypeptide and the surrounding solvent contribute to $\Delta\Delta S$ and $\Delta\Delta H$ in a complex manner with compensatory effects (*20*, *32*).

DISCUSSION

Stability Analysis. We report herein quantitative equilibrium analysis of thermodynamics for apo SODs using GdmCl curves as well as DSC. We demonstrate that apo SODs undergo reversible denaturation in GdmCl, which is well fit by a 3-state model with monomer intermediate (Figures 2, 3, and 5). The intermediate is increasingly populated with decreasing protein concentration, as evidenced by increasingly biphasic character in GdmCl curves, whereas the transition approaches a monophasic 2-state transition at

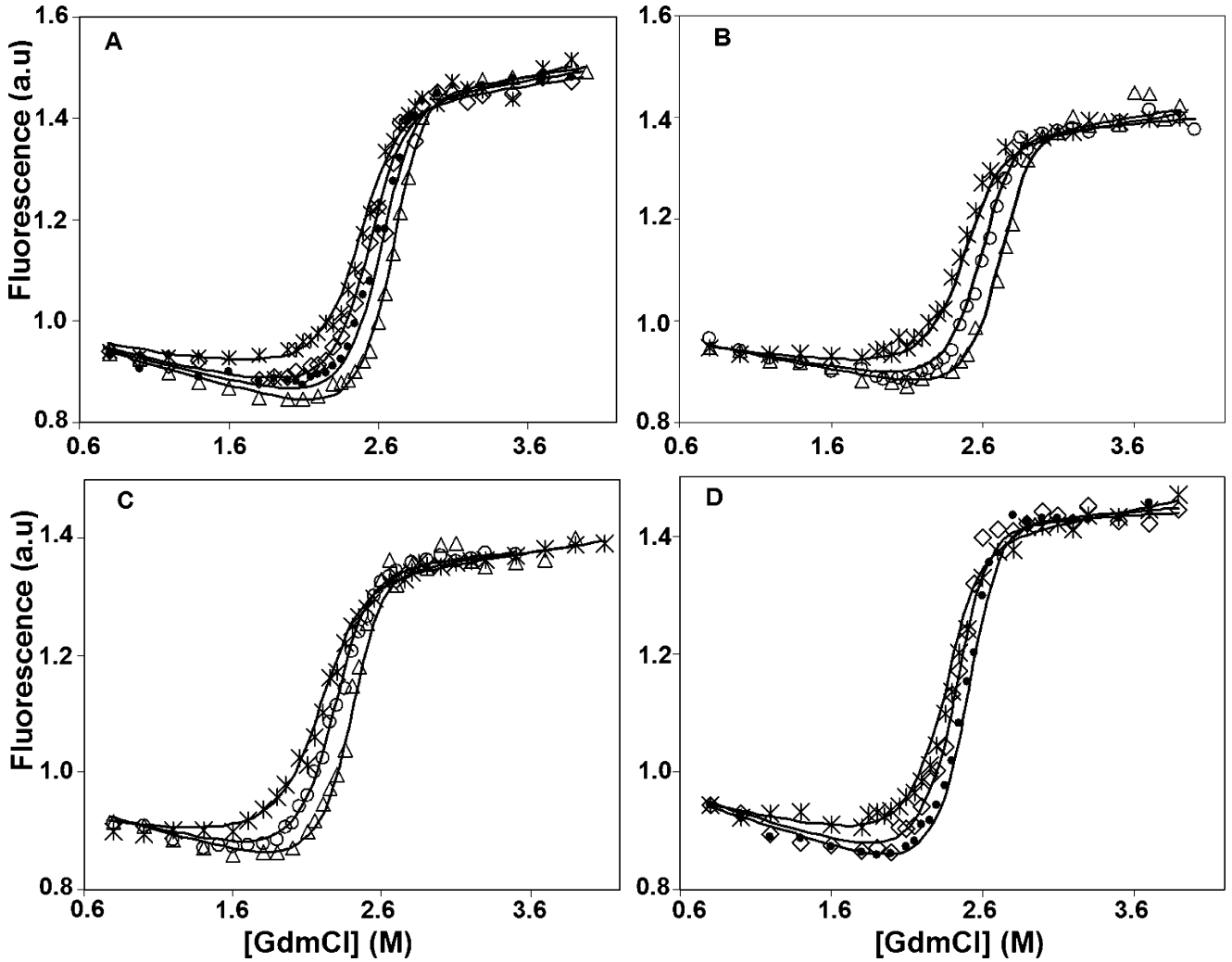

FIGURE 5: Concentration dependence of equilibrium unfolding of apo pseudoWT mutants: (A) E100G, (B) G85R, (C) I113T, and (D) G93R, measured by fluorescence. Protein concentrations shown are 1 μM (*), 3 μM (◇), 5 μM (○), 10 μM (●), and 30 μM (△). Measurements were performed at 25 °C, 20 mM HEPES pH 7.8 with 0.75 M sodium sulfate. Data are normalized, and scaled for protein concentration for ease of comparison. As was the case for pseudoWT, data points below 0.8 M GdmCl were not fit due to nonlinear effects and are excluded for the sake of clarity. The lines represent global fits to a 3-state model with a monomer intermediate. Fitted values for ΔGs and *m*s from fluorescence measurements agree well with values obtained from circular dichroism measurements at 216 and 231 nm (Table 1).

increased protein concentration (Figures 2 and 3). A 3-state transition with a monomer intermediate was also reported for GdmCl studies of holo SODs (*19*) and copper-depleted SOD (*33*). The observation of the monomer intermediate for apo SOD is physically reasonable, given that the dimer interface is variable among SODs from different organisms, and *Escherichia coli* SOD is a natural monomer (*34*−*36*). Furthermore, an engineered monomeric variant of apo SOD is folded (*37*) and a monomer intermediate is observed in kinetic experiments (*17*). Monomer intermediate formation for apo and holo SOD is not detected by DSC, likely related to the relatively high protein concentrations for these experiments, for which data can be fit using a dimer 2-state transition (*20*). Thus, DSC can be used to analyze only ΔG_{total}, whereas global fitting of the GdmCl curves as a function of protein concentration allows ΔG_{total} to be deconvoluted for simultaneous measurement of both dimer dissociation (ΔG_1) and monomer intermediate stability (ΔG_2).

There is very good agreement for ΔG_{total} measured by GdmCl denaturation and by DSC for apo pseudoWT (~16.0 and 15.8 kcal (mol dimer)$^{-1}$, respectively, Tables 1 and 3). Oliveberg and co-workers have reported a similar value for ΔG_{total} determined by urea denaturation, but did not show any equilibrium data in their primarily kinetic study (*17*). The value of ΔG_1 measured here for apo pseudoWT (12.8 kcal (mol dimer)$^{-1}$, Table 1) is consistent with analytical ultracentrifugation data at pH 5.5 which estimated $K_d < 10^{-8}$ M for apo and holo wild-type SOD, corresponding to a ΔG_1 of >10.9 kcal (mol dimer)$^{-1}$ (*38*). A very similar value for ΔG_1 of ~13 kcal (mol dimer)$^{-1}$ was also obtained by GdmCl denaturation curves for holo pseudoWT (*19*). These comparisons provide further evidence that pseudoWT is a good model for wild-type, and that the free energy values obtained from the GdmCl curves are reliable. Also, the GdmCl experiments provide new quantitative data that metal binding has little effect on dimer association.

Effects of Sodium Sulfate. Sodium sulfate is known to stabilize proteins via a mechanism of preferential exclusion of salt ions from the protein solvent sphere (*39*), and to enhance the population of kinetic folding intermediates (*30*, *40*, *41*). There is, however, little quantitative data on the effects of sodium sulfate on the stability of equilibrium intermediates. The extent of sodium sulfate mediated protein

Table 2: DSC Dimer 2-State Fitted Parameters for Apo SODs

protein	[protein] (mg mL^{-1})	t_m (°C)	ΔH_{vH}[b] (kcal (mol dimer)$^{-1}$)	$\Delta H_{vH}/\Delta H_{cal}$	ΔC_p[c] (kcal (mol dimer)$^{-1}$ °C^{-1})
PWT[a]	3.00	61.9 ± 0.0	183.3 ± 1.9	1.44	3.93
PWT[a]	2.99	61.3 ± 0.0	178.5 ± 1.4	1.00	5.11
PWT[a]	1.50	60.3 ± 0.0	164.3 ± 4.0	1.09	5.11
PWT[a]	1.42	60.0 ± 0.0	163.6 ± 2.4	0.96	4.38
PWT[a]	0.73	58.8 ± 0.0	144.4 ± 2.5	0.94	4.30
PWT[a]	0.44	59.1 ± 0.2	137.6 ± 9.4	0.96	4.25
PWT[a]	0.27	57.8 ± 0.2	115.4 ± 2.7	0.78	3.85
PWT[a]	0.21	58.4 ± 0.1	116.7 ± 9.1	0.84	3.74
PWT[a]	0.20	58.3 ± 0.1	112.8 ± 6.7	1.02	2.95
PWT[a]	0.05	57.8 ± 0.6	106.5 ± 18.9	0.97	3.71
			mean ± SD[d]:	1.00 ± 0.18	4.13 ± 0.65
G85R	0.50	55.1 ± 0.0	160.8 ± 3.6	1.54	4.32
G85R	0.43	54.9 ± 0.0	166.5 ± 2.1	1.90	3.56
G85R	0.17	54.0 ± 0.1	158.2 ± 6.0	1.37	4.12
E100G	1.20	53.1 ± 0.0	184.7 ± 2.0	1.83	1.82
E100G	0.50	51.0 ± 0.0	163.6 ± 2.3	1.51	2.18
E100G	0.20	49.5 ± 0.0	156.9 ± 3.5	1.79	2.40
G93R[a]	0.40	48.5 ± 0.0	144.0 ± 2.4	1.20	4.30
G93R[a]	0.21	47.1 ± 0.0	123.7 ± 2.7	1.22	5.73
G93R[a]	0.21	46.8 ± 0.1	115.4 ± 3.7	1.22	6.14
I113T	0.75	46.3 ± 0.0	118.0 ± 2.0	1.25	4.80
I113T	0.50	47.1 ± 0.1	129.0 ± 4.1	1.37	2.78
I113T	0.40	46.0 ± 0.1	106.2 ± 4.0	0.87	4.62
I113T	0.10	45.3 ± 1.0	105.3 ± 18.1	1.19	1.85
			mean ± SD[d]:	1.40 ± 0.30	3.74 ± 1.45

[a] Data taken from ref *20*. [b] ΔH_{vH} errors (±) were propagated according to standard procedures (*67*) from fitted errors for Δh and β. [c] ΔC_p errors for individual fits could not be reliably calculated since they are based on uncertainties of five different variables. [d] SD, standard deviation.

Table 3: Summary of Thermodynamic Parameters of PseudoWT and Mutant Apo SODs by DSC and GdmCl Curve Analysis

protein	t_m[a] (°C)	Δt_m[b] (°C)	$\Delta G_{total}(t_{av})$[c] (kcal (mol dimer)$^{-1}$)	ΔG_{total}(25°C)[d] (kcal (mol dimer)$^{-1}$)	ΔG_1[e] (kcal (mol dimer)$^{-1}$)	ΔG_2[e] (kcal (mol monomer)$^{-1}$)	ΔG_{total}[f] (kcal (mol dimer)$^{-1}$)	$\Delta\Delta H$[g] (kcal (mol dimer)$^{-1}$)	$\Delta\Delta S$[h] (kcal (mol dimer)$^{-1}$ K^{-1})	$\Delta\Delta G_1$[i] (kcal (mol dimer)$^{-1}$)	$\Delta\Delta G_2$[j] (kcal (mol monomer)$^{-1}$)	$\Delta\Delta G_{total}$[k] (kcal (mol dimer)$^{-1}$)	$\Delta\Delta G_{total}(t_{av})$[l] (kcal (mol dimer)$^{-1}$)
PWT	59.0	na[m]	10.2 ± 0.6 *10.1 ± 0.5*	17.3 ± 2.4 *15.8 ± 2.4*	12.1 ± 0.2	10.3 ± 0.2	32.8 ± 0.1	na[m]	na[m]	na[m]	na[m]	na[m]	na[m]
G85R	55.2	−3.8	8.6 ± 0.1 *8.5 ± 0.1*	16.9 ± 0.3 *15.7 ± 0.3*	11.6 ± 0.1	8.5 ± 0.1	28.7 ± 0.2	+13.3	+0.046	−0.5	−1.8	−4.1	−1.6 *−1.6*
E100G	51.3	−7.7	6.6 ± 0.4 *6.6 ± 0.4*	16.6 ± 1.0 *15.6 ± 1.0*	11.2 ± 0.2	8.5 ± 0.2	28.2 ± 0.1	+31.3	+0.107	−0.9	−1.8	−4.6	−3.6 *−3.5*
G93R	48.9	−10.1	5.7 ± 0.2 *5.6 ± 0.2*	13.5 ± 1.0 *12.7 ± 1.0*	11.8 ± 0.2	7.8 ± 0.1	27.4 ± 0.1	+4.4	+0.027	−0.3	−2.5	−5.4	−4.5 *−4.5*
I113T	46.8	−12.2	5.0 ± 0.5 *5.0 ± 0.5*	12.0 ± 0.6 *11.3 ± 0.6*	10.8 ± 0.2	7.6 ± 0.1	26.0 ± 0.3	−5.8	−0.002	−1.3	−2.7	−6.8	−5.2 *−5.2*

[a] t_m was determined at 0.50 mg mL^{-1} using average stability plots (ΔG vs temperature (*20*)) generated from the parameters listed in Table 2. [b] Change in the t_m of the mutant relative to pseudoWT at 0.50 mg mL^{-1}, calculated as $t_m^{mutant} - t_m^{pseudoWT}$. [c] $\Delta G_{total}(t_{av})$ obtained from DSC analysis. $t_{av} = 52.3$ °C is the average of the t_m values for 0.50 mg mL^{-1} protein. Values were extrapolated to the t_{av} using a temperature-independent ΔC_p. Italicized values were extrapolated using a temperature-dependent ΔC_p as previously described (*20*). Errors (±) are standard deviations from multiple datasets listed in Table 2. [d] ΔG_{total}(25°C) obtained from DSC analysis. Values were extrapolated to 25 °C using a temperature-independent ΔC_p. Italicized values were extrapolated using a temperature-dependent ΔC_p as previously described (*20*). Errors (±) are standard deviations from multiple datasets listed in Table 2. [e] ΔG_1 and ΔG_2 are derived from 3-state monomer intermediate global fitting of GdmCl curves in 0.75 M Na_2SO_4 (Table 1). Values are an average of fitted values from three probes (CD 216 nm, CD 231 nm, and fluorescence). Errors (±) are standard deviations from averaging the three probes. [f] $\Delta G_{total} = \Delta G_1 + 2\Delta G_2$. Errors (±) are standard deviations from averaging the three probes. [g] $\Delta\Delta H = \Delta H^{mutant} - \Delta H^{pseudoWT}$. Values are obtained from DSC and calculated using the temperature-independent ΔC_p. [h] $\Delta\Delta S = \Delta S^{mutant} - \Delta S^{pseudoWT}$. Values are obtained from DSC and are calculated using the temperature-independent ΔC_p. [i] $\Delta\Delta G_1 = \Delta G_1^{mutant} - \Delta G_1^{pseudoWT}$. [j] $\Delta\Delta G_2 = \Delta G_2^{mutant} - \Delta G_2^{pseudoWT}$. [k] $\Delta\Delta G_{total} = \Delta G^{mutant} - \Delta G^{pseudoWT}$. Values are derived from 3-state monomer intermediate fits of GdmCl denaturation curves; negative value indicates that the mutant SOD is destabilized relative to the pseudoWT. [l] $\Delta\Delta G_{total}(t_{av}) = \Delta G_{total(tav)}^{mutant} - \Delta G_{total(tav)}^{pseudoWT}$. The values are derived from DSC analysis using ΔGs calculated at the t_{av} which are more accurate than values obtained at 25 °C due to a shorter extrapolation (*20*). [m] Not applicable.

stabilization is related to solvent accessible surface area. Unfolding of the apo SOD monomer intermediate produces a larger change in surface area than does dimer dissociation, based on the higher *m* value for the former (*42*) and structural data (*43*). Consistent with these changes, sodium sulfate causes a relatively large stabilization of the monomer intermediate with little effect on dimerization. It is interesting that sodium sulfate causes a decrease in the m_1 value while increasing m_2 (see Results). This suggests that sodium sulfate also causes significant compaction of the apo monomer intermediate; structural studies conducted on a monomeric variant of apo SOD have shown it to be less compact and

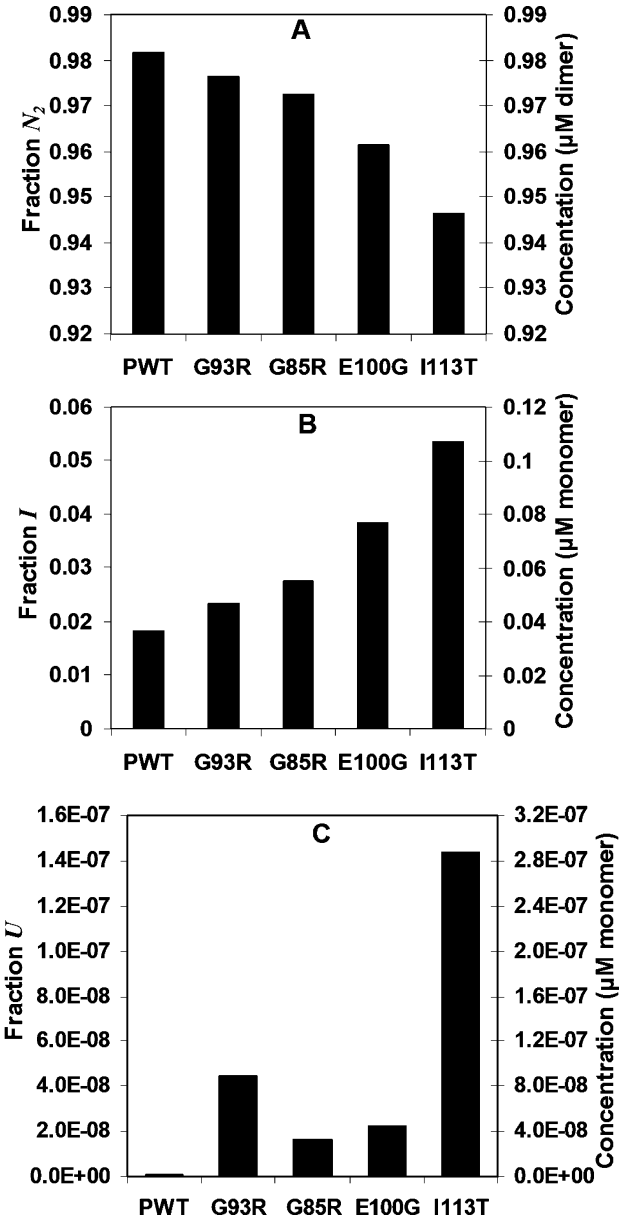

FIGURE 6: Relative fractions and concentrations of the different species present at equilibrium for 1 μM apo pseudoWT and mutants in 0.75 M sodium sulfate and 0 M GdmCl. Mutations in SOD result in a decrease in the fraction and concentration of (A) the native state with corresponding increases in (B) the folded monomer intermediate and larger increases in (C) the unfolded monomer.

more flexible than holo (*37*). Compaction of poorly structured states by sodium sulfate has also been observed for other proteins (*40*, *44*, *45*).

The experiments reported herein for apo SODs demonstrate that sodium sulfate can be used to facilitate measurements of the determinants of intermediate stability. The similarity of the changes in overall stability measured by chemical denaturation in sodium sulfate and by DSC in the absence of sodium sulfate further validates the former approach, which may be useful for the study of intermediates in other systems. It is worth noting that the changes in stability measured in sodium sulfate are slightly larger than those measured by DSC (Table 3). Similarly, trehalose also tended to increase the free energy changes caused by mutations (*46*). This leads to the interesting observation that small molecule stabilizers not only enhance net protein

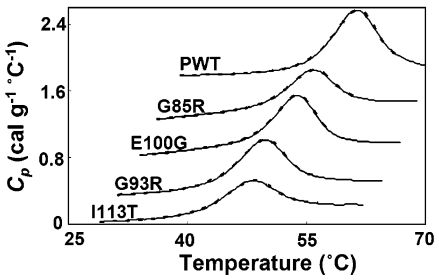

FIGURE 7: DSC data (excess specific heat absorption, C_p, versus temperature) of apo pseudoWT and apo mutants. Typical thermograms (—) with corresponding dimer 2-state ($N_2 \leftrightharpoons 2U$) fits (- - -) are shown. Protein concentrations are 1.50, 0.43, 1.20, 0.40, and 0.75 mg mL^{-1} for pseudoWT (PWT), G85R, E100G, G93R, and I113T, respectively. Datasets are offset for clarity.

stability but also enhance the effects of individual amino acids on stability. It is also worth pointing out that the measurements of stability and stability changes made in the presence of stabilizing agents may actually be more biologically relevant than measurements made in dilute buffers, since the cellular environment has high ionic strength and high concentrations of molecules which may increase protein stability (*47*−*49*).

Effects of Mutations. The SOD mutants studied here are chemically and structurally diverse (Figure 1) and all have decreased thermodynamic stability. This is not necessarily expected, given the structural contexts of the mutations (see below) and previous findings that not all ALS-associated apo SODs are destabilizing. For example, the metal binding mutants H46R and D124V have been shown to have apparent t_ms that are actually slightly higher than apo wild-type, while the non metal binding mutant D101N has virtually identical apparent t_m (*16*). The observations reported in this study are similar to other measurements for these mutants, with some significant differences. The apparent t_ms for the irreversible thermal unfolding of all four mutants in a wild-type background are ~4−11 °C lower (*16*) than values obtained here (Table 2); although the rank order of t_ms is generally similar, E100G is much more destabilized in the wild-type background. The apparent t_ms may differ from the results here due to effects of irreversible unfolding/aggregation, and so may not consistently reflect differences in thermodynamic stability (*14*, *50*). Estimates of free energies based on kinetic measurements in urea using pseudoWT and monomeric variant backgrounds (*18*) are in the same range as values reported here, although not generally in close agreement. On the one hand, this may not be surprising, considering experimental uncertainties in measurements. On the other hand, the differences may be real due to the different approaches used, e.g. effects of mutations may be different in the monomeric variant than in pseudoWT, and there may be errors in the assumptions made in the kinetic analysis. Since we obtain consistent results using two equilibrium approaches, changes in stability are likely measured more accurately using the equilibrium methods.

It is instructive to consider the effects of the individual mutations. Mutation of G85 to R substitutes a conserved glycine, located near the edge of the active site in a β-bulge within strand 5, with a basic residue. This mutation occurs at a fairly solvent exposed site and causes relatively small localized structural changes in yeast SOD (Hart, P. J.,

Ogihara, N. L., Liu, H., Nersissian, A. M., Valentine, J. S., Eisenberg, D. (pdb code 1F18)). Altered metal binding may be a significant factor in the decreased stability of holo G85R (*19*). Considering also that other metal binding mutations have been found to have relatively small effects on apo stability (*16*), apo G85R may be expected to exhibit relatively little change in stability. Consistent with this, G85R is the least destabilized of the mutants studied here; however, it is nevertheless significantly destabilized. Mutation of E100 to G could be expected to be destabilizing due to the loss of a favorable electrostatic interaction with K30 and increased entropy of the unfolded state (*19*). G93 is highly conserved at position $i+3$ of a tight turn (*51*). This wild-type backbone conformation is not readily accommodated by other residues; consequently mutations to R and other residues are all destabilizing (Table 3) (*20*). Unlike G85R, E100G, and G93R, which are relatively far from the dimer interface, I113 is located in a hydrophobic patch on the monomer surface, at the edge of the dimer interface. Mutation to T substitutes a more hydrophilic residue, causing the largest change in ΔG_1, as might be expected. Rather unexpectedly, the mutation also markedly decreases monomer intermediate stability, despite substituting a more polar residue at the monomer surface. The destabilization may result from decreased packing and hence increased exposure of the hydrophobic residues surrounding position 113. Thus, overall, the mutations studied here destabilize SOD, largely by decreasing monomer intermediate stability (ΔG_2), but also tend to weaken dimer association (ΔG_1), even for mutations that are relatively distant from the dimer interface.

A particularly interesting observation is that, in contrast to the results obtained here for apo G85R and E100G, these mutations do not clearly decrease ΔG_1 for the holo proteins (*19*). This suggests that the effects of mutations may tend to propagate more in apo than in holo. Compaction with concomitant increase in stability resulting from SOD metal binding may cause the effects of mutations to be more localized. The DSC data reported here (Table 2) extend our previous observation by DSC on other SOD mutants that the apo proteins have an increased tendency to aggregate (*20*), which are further corroborated by light scattering measurements (*14*, *18*, *20*). The lower stability and enhanced flexibility of apo SOD may be important for facilitating aggregation.

Disease Implication. It is particularly striking that all ALS-associated SOD mutations studied to date appear to decrease the stability of holo SOD, and usually also of apo SOD (*14*−*16*, *18*−*20*). This implicates decreased stability as a key factor in causing disease. Destabilizing mutations have been proposed to cause increased toxic aggregation not only in ALS but also in many other protein misfolding diseases (*7*−*9*). Decreased stability of apo mutant SOD, modulated by differences in protein net charge, has been proposed to be correlated with shorter ALS disease duration (*18*). Data from this study on G85R, E100G, and I113T appear to fit this reported correlation (*52*, *53*). G93R, which has been shown in limited studies to have large variations in disease duration (*54*), could not be evaluated due to insufficient published patient data. It is noteworthy that there is considerable scatter in the previously reported correlation, and data for additional mutants do not necessarily follow the trend (e.g. G37R (*16*, *55*) and some G93 mutations (*20*, *52*, *53*, *56*, *57*)). Analysis of such correlations, and possible additional modulating factors (*58*), may be hampered by experimental uncertainties in protein stabilities assessed by kinetics or apparent t_ms. This re-emphasizes the need for accurate equilibrium stability measurements, not only for apo but also for holo SODs, whose destabilization has also be implicated in toxic aggregation (*16*, *19*, *59*, *60*).

Stability data may also provide important information for understanding disease mechanism, such as elucidating which states of the protein may be aggregating. In general, aggregation is thought to arise from the increased population by mutant proteins of partially folded aggregation-prone species (*61*). In the case of transthyretin, associated with familial amyloid polyneuropathy, the native tetramer must dissociate to monomers and then partially unfold to form the aggregation-prone species (*62*, *63*). Similar dissociation and partial unfolding may also be required for aggregation of either holo or apo SOD mutants (*14*, *18*, *19*, *59*, *60*, *64*). In this regard, it is noteworthy that the populations of the monomer intermediate and the unfolded monomer are increased for all the apo mutants (Figure 6). Either species could promote SOD aggregation in ALS.

In conclusion, we have conducted systematic, quantitative studies of the relative stabilities of different conformational states for apo and previously for holo SODs (*19*), and the effects of mutations on these states. These studies are of fundamental interest for understanding folding and stability of this complex dimeric metalloenzyme. Furthermore, we have established methodology and obtained important data for further investigation of aggregation mechanisms in ALS, which may ultimately contribute to development of urgently needed strategies to combat the disease, for example, using drug binding to decrease the population of aggregation-prone states (*65*, *66*).

ACKNOWLEDGMENT

We would like to thank Colin Campbell for assistance with Matlab as well as Kristin Dimmick and Jarrod Johnson for experimental assistance.

REFERENCES

1. Rosen, D. R. (1993) Mutations in Cu/Zn superoxide dismutase gene are associated with familial amyotrophic lateral sclerosis, *Nature 364*, 362.
2. Rowland, L. P., and Shneider, N. A. (2001) Amyotrophic lateral sclerosis, *N. Engl. J. Med. 344*, 1688−1700.
3. Tainer, J. A., Getzoff, E. D., Beem, K. M., Richardson, J. S., and Richardson, D. C. (1982) Determination and analysis of the 2 A-structure of copper, zinc superoxide dismutase, *J. Mol. Biol. 160*, 181−217.
4. Richardson, J., Thomas, K. A., Rubin, B. H., and Richardson, D. C. (1975) Crystal structure of bovine Cu,Zn superoxide dismutase at 3 Å resolution: chain tracing and metal ligands, *Proc. Natl. Acad. Sci. U.S.A. 72*, 1349−1353.
5. Radunovic, A., and Leigh, P. N. (1999) ALSODatabase: database of SOD1 (and other) gene mutations in ALS on the Internet. European FALS Group and ALSOD Consortium, *Amyotrophic Lateral Scler. Other Mot. Neuron Disord. 1*, 45−49.
6. Julien, J. P. (2001) Amyotrophic lateral sclerosis. Unfolding the toxicity of the misfolded, *Cell 104*, 581−591.
7. Valentine, J. S., Doucette, P. A., and Potter, S. Z. (2005) Copper-Zinc Superoxide Dismutase and Amyotrophic Lateral Sclerosis, *Annu. Rev. Biochem. 74*, 563−593.
8. Bendotti, C., and Carri, M. T. (2004) Lessons from models of SOD1-linked familial ALS, *Trends Mol. Med. 10*, 393−400.

9. Gregersen, N., Bolund, L., and Bross, P. (2005) Protein misfolding, aggregation, and degradation in disease, *Mol. Biotechnol. 31*, 141−150.
10. Lepock, J. R., Frey, H. E., and Hallewell, R. A. (1990) Contribution of conformational stability and reversibility of unfolding to the increased thermostability of human and bovine superoxide dismutase mutated at free cysteines, *J. Biol. Chem. 265*, 21612−21618.
11. Hallewell, R. A., Imlay, K. C., Lee, P., Fong, N. M., Gallegos, C., Getzoff, E. D., Tainer, J. A., Cabelli, D. E., Tekamp-Olson, P., Mullenbach, G. T., and et al. (1991) Thermostabilization of recombinant human and bovine CuZn superoxide dismutases by replacement of free cysteines, *Biochem. Biophys. Res. Commun. 181*, 474−480.
12. Parge, H. E., Hallewell, R. A., and Tainer, J. A. (1992) Atomic structures of wild-type and thermostable mutant recombinant human Cu,Zn superoxide dismutase, *Proc. Natl. Acad. Sci. U.S.A. 89*, 6109−6113.
13. McRee, D. E., Redford, S. M., Getzoff, E. D., Lepock, J. R., Hallewell, R. A., and Tainer, J. A. (1990) Changes in crystallographic structure and thermostability of a Cu,Zn superoxide dismutase mutant resulting from the removal of a buried cysteine, *J. Biol. Chem. 265*, 14234−14241.
14. Stathopulos, P. B., Rumfeldt, J. A., Scholz, G. A., Irani, R. A., Frey, H. E., Hallewell, R. A., Lepock, J. R., and Meiering, E. M. (2003) Cu/Zn superoxide dismutase mutants associated with amyotrophic lateral sclerosis show enhanced formation of aggregates in vitro, *Proc. Natl. Acad. Sci. U.S.A. 100*, 7021−7026.
15. Rodriguez, J. A., Valentine, J. S., Eggers, D. K., Roe, J. A., Tiwari, A., Brown, R. H., Jr., and Hayward, L. J. (2002) Familial amyotrophic lateral sclerosis-associated mutations decrease the thermal stability of distinctly metallated species of human copper/zinc superoxide dismutase, *J. Biol. Chem. 277*, 15932−15937.
16. Rodriguez, J. A., Shaw, B. F., Durazo, A., Sohn, S. H., Doucette, P. A., Nersissian, A. M., Faull, K. F., Eggers, D. K., Tiwari, A., Hayward, L. J., and Valentine, J. S. (2005) Destabilization of apoprotein is insufficient to explain Cu,Zn-superoxide dismutase-linked ALS pathogenesis, *Proc. Natl. Acad. Sci. U.S.A. 102*, 10516−10521.
17. Lindberg, M. J., Normark, J., Holmgren, A., and Oliveberg, M. (2004) Folding of human superoxide dismutase: disulfide reduction prevents dimerization and produces marginally stable monomers, *Proc. Natl. Acad. Sci. U.S.A. 101*, 15893−15898.
18. Lindberg, M. J., Bystrom, R., Boknas, N., Andersen, P. M., and Oliveberg, M. (2005) Systematically perturbed folding patterns of amyotrophic lateral sclerosis (ALS)-associated SOD1 mutants, *Proc. Natl. Acad. Sci. U.S.A. 102*, 9754−9759.
19. Rumfeldt, J. A., Stathopulos, P. B., Chakrabarrty, A., Lepock, J. R., and Meiering, E. M. (2006) Mechanism and Thermodynamics of Guanidinium Chloride-induced Denaturation of ALS-associated Mutant Cu,Zn Superoxide Dismutases, *J. Mol. Biol. 355*, 106−123.
20. Stathopulos, P. B., Rumfedt, J. A. O., Karbassi, F., Sidall, C., Lepock, J. R., and Meiering, E. M. (2006) Calorimetric analysis of thermodynamic stability and aggregation for apo and holo ALS-associated GLY93 mutants of superoxide dismutase, *J. Biol. Chem. 281*, 6184−6193.
21. Getzoff, E. D., Cabelli, D. E., Fisher, C. L., Parge, H. E., Viezzoli, M. S., Banci, L., and Hallewell, R. A. (1992) Faster superoxide dismutase mutants designed by enhancing electrostatic guidance, *Nature 358*, 347−351.
22. Furukawa, Y., and O'Halloran T, V. (2005) ALS mutations have the greatest destabilizing effect on the apo, reduced form of SOD1, leading to unfolding and oxidative aggregation, *J. Biol. Chem. 3*, 3.
23. McCord, J. M., and Fridovich, I. (1969) Superoxide dismutase. An enzymic function for erythrocuprein (hemocuprein), *J. Biol. Chem. 244*, 6049−6055.
24. Lowry, O. H., Rosenbrough, N. J., Farr, L. A., and Randal, R. J. (1951) Protein measurement with the folin phenol reagent, *J. Biol. Chem. 193*, 265−275.
25. Sturtevant, J. M. (1987) Biochemical applications of differential scanning calorimetry, *Annu. Rev. Phys. Chem. 38*, 463−488.
26. Privalov, P. L., and Potekhin, S. A. (1986) Scanning microcalorimetry in studying temperature-induced changes in proteins, *Methods Enzymol. 131*, 4−51.
27. Park, Y. C., and Bedouelle, H. (1998) Dimeric tyrosyl-tRNA synthetase from Bacillus stearothermophilus unfolds through a monomeric intermediate. A quantitative analysis under equilibrium conditions, *J. Biol. Chem. 273*, 18052−18059.
28. Spudich, G., and Marqusee, S. (2000) A change in the apparent m value reveals a populated intermediate under equilibrium conditions in *Escherichia coli* ribonuclease HI, *Biochemistry 39*, 11677−11683.
29. Timasheff, S. N. (1998) Control of protein stability and reactions by weakly interacting cosolvents: the simplicity of the complicated, *Adv. Protein Chem. 51*, 355−432.
30. Ferguson, N., Capaldi, A. P., James, R., Kleanthous, C., and Radford, S. E. (1999) Rapid folding with and without populated intermediates in the homologous four-helix proteins Im7 and Im9, *J. Mol. Biol. 286*, 1597−1608.
31. Lepock, J. R., Ritchie, K. P., Kolios, M. C., Rodahl, A. M., Heinz, K. A., and Kruuv, J. (1992) Influence of transition rates and scan rate on kinetic simulations of differential scanning calorimetry profiles of reversible and irreversible protein denaturation, *Biochemistry 31*, 12706−12712.
32. Sturtevant, J. M. (1994) The thermodynamic effects of protein mutations, *Curr. Opin. Struct. Biol. 4*, 69−78.
33. Stroppolo, M. E., Malvezzi-Campeggi, F., Mei, G., Rosato, N., and Desideri, A. (2000) Role of the tertiary and quaternary structures in the stability of dimeric copper, zinc superoxide dismutases, *Arch. Biochem. Biophys. 377*, 215−218.
34. Bordo, D., Matak, D., Djinovic-Carugo, K., Rosano, C., Pesce, A., Bolognesi, M., Stroppolo, M. E., Falconi, M., Battistoni, A., and Desideri, A. (1999) Evolutionary constraints for dimer formation in prokaryotic Cu,Zn superoxide dismutase, *J. Mol. Biol. 285*, 283−296.
35. Bourne, Y., Redford, S. M., Steinman, H. M., Lepock, J. R., Tainer, J. A., and Getzoff, E. D. (1996) Novel dimeric interface and electrostatic recognition in bacterial Cu,Zn superoxide dismutase, *Proc. Natl. Acad. Sci. U.S.A. 93*, 12774−12779.
36. Pesce, A., Capasso, C., Battistoni, A., Folcarelli, S., Rotilio, G., Desideri, A., and Bolognesi, M. (1997) Unique structural features of the monomeric Cu,Zn superoxide dismutase from Escherichia coli, revealed by X-ray crystallography, *J. Mol. Biol. 274*, 408−420.
37. Banci, L., Bertini, I., Cramaro, F., Del Conte, R., and Viezzoli, M. S. (2003) Solution structure of Apo Cu,Zn superoxide dismutase: role of metal ions in protein folding, *Biochemistry 42*, 9543−9553.
38. Doucette, P. A., Whitson, L. J., Cao, X., Schirf, V., Demeler, B., Valentine, J. S., Hansen, J. C., and Hart, P. J. (2004) Dissociation of human copper-zinc superoxide dismutase dimers using chaotrope and reductant. Insights into the molecular basis for dimer stability, *J. Biol. Chem. 279*, 54558−54566.
39. Timasheff, S. N. (2002) Protein hydration, thermodynamic binding, and preferential hydration, *Biochemistry 41*, 13473−13482.
40. Rami, B. R., and Udgaonkar, J. B. (2002) Mechanism of formation of a productive molten globule form of barstar, *Biochemistry. 41*, 1710−1716.
41. Sauder, J. M., MacKenzie, N. E., and Roder, H. (1996) Kinetic mechanism of folding and unfolding of Rhodobacter capsulatus cytochrome c2, *Biochemistry 35*, 16852−16862.
42. Myers, J. K., Pace, C. N., and Scholtz, J. M. (1995) Denaturant m values and heat capacity changes: relation to changes in accessible surface areas of protein unfolding, *Protein Sci. 4*, 2138−2148.
43. Strange, R. W., Antonyuk, S., Hough, M. A., Doucette, P. A., Rodriguez, J. A., Hart, P. J., Hayward, L. J., Valentine, J. S., and Hasnain, S. S. (2003) The structure of holo and metal-deficient wild-type human Cu, Zn superoxide dismutase and its relevance to familial amyotrophic lateral sclerosis, *J. Mol. Biol. 328*, 877−891.
44. Nishimura, C., Uversky, V. N., and Fink, A. L. (2001) Effect of salts on the stability and folding of staphylococcal nuclease, *Biochemistry 40*, 2113−2128.
45. Cerasoli, E., Kelly, S. M., Coggins, J. R., Lapthorn, A. J., Clarke, D. T., and Price, N. C. (2003) Effects of salts on the function and conformational stability of shikimate kinase, *Biochim. Biophys. Acta 1648*, 43−54.
46. Chen, L., Cabrita, G. J., Otzen, D. E., and Melo, E. P. (2005) Stabilization of the ribosomal protein S6 by trehalose is counterbalanced by the formation of a putative off-pathway species, *J. Mol. Biol. 351*, 402−416.
47. Bolen, D. W., and Baskakov, I. V. (2001) The osmophobic effect: natural selection of a thermodynamic force in protein folding, *J. Mol. Biol. 310*, 955−963.

48. Chamberlin, M. E., and Strange, K. (1989) Anisosmotic cell volume regulation: a comparative view, *Am. J. Physiol. 257*, C159−C173.
49. Somero, G. N. (1986) Protons, osmolytes, and fitness of internal milieu for protein function, *Am. J. Physiol. 251*, R197−R213.
50. Chrunyk, B. A., and Wetzel, R. (1993) Breakdown in the relationship between thermal and thermodynamic stability in an interleukin-1 beta point mutant modified in a surface loop, *Protein Eng. 6*, 733−738.
51. Bordo, D., Djinovic, K., and Bolognesi, M. (1994) Conserved patterns in the Cu,Zn superoxide dismutase family, *J. Mol. Biol. 238*, 366−386.
52. Juneja, T., Pericak-Vance, M. A., Laing, N. G., Dave, S., and Siddique, T. (1997) Prognosis in familial amyotrophic lateral sclerosis: progression and survival in patients with glu100gly and ala4val mutations in Cu,Zn superoxide dismutase, *Neurology 48*, 55−57.
53. Cudkowicz, M. E., McKenna-Yasek, D., Sapp, P. E., Chin, W., Geller, B., Hayden, D. L., Schoenfeld, D. A., Hosler, B. A., Horvitz, H. R., and Brown, R. H. (1997) Epidemiology of mutations in superoxide dismutase in amyotrophic lateral sclerosis, *Ann. Neurol. 41*, 210−221.
54. Orrell, R. W., Habgood, J. J., Gardiner, I., King, A. W., Bowe, F. A., Hallewell, R. A., Marklund, S. L., Greenwood, J., Lane, R. J., and deBelleroche, J. (1997) Clinical and functional investigation of 10 missense mutations and a novel frameshift insertion mutation of the gene for copper−zinc superoxide dismutase in UK families with amyotrophic lateral sclerosis, *Neurology 48*, 746−751.
55. Lindberg, M. (2004) Protein folding studies of human superoxide dismutase and ALS associated mutants, Ph.D. Thesis, Department of Biochemistry, Umea University, Umea.
56. Iwai, K., Yamamoto, M., Yoshihara, T., and Sobue, G. (2002) Anticipation in familial amyotrophic lateral sclerosis with SOD1-G93S mutation, *J. Neurol. Neurosurg. Psychiatry 72*, 819−820.
57. Orrell, R. W., Habgood, J. J., Malaspina, A., Mitchell, J., Greenwood, J., Lane, R. J., and deBelleroche, J. S. (1999) Clinical characteristics of SOD1 gene mutations in UK families with ALS, *J. Neurol. Sci. 169*, 56−60.
58. Chiti, F., Stefani, M., Taddei, N., Ramponi, G., and Dobson, C. M. (2003) Rationalization of the effects of mutations on peptide and protein aggregation rates, *Nature 424*, 805−808.
59. Hough, M. A., Grossmann, J. G., Antonyuk, S. V., Strange, R. W., Doucette, P. A., Rodriguez, J. A., Whitson, L. J., Hart, P. J., Hayward, L. J., Valentine, J. S., and Hasnain, S. S. (2004) Dimer destabilization in superoxide dismutase may result in disease-causing properties: structures of motor neuron disease mutants, *Proc. Natl. Acad. Sci. U.S.A. 101*, 5976−5981.
60. Banci, L., Bertini, I., D'Amelio, N., Gaggelli, E., Libralesso, E., Matecko, I., Turano, P., and Valentine, J. S. (2005) Fully metallated S134N Cu,Zn-superoxide dismutase displays abnormal mobility and intermolecular contacts in solution, *J. Biol. Chem. 280*, 35815−35821.
61. Chow, M. K., Lomas, D. A., and Bottomley, S. P. (2004) Promiscuous beta-strand interactions and the conformational diseases, *Curr. Med. Chem. 11*, 491−499.
62. Damas, A. M., and Saraiva, M. J. (2000) Review: TTR amyloidosis-structural features leading to protein aggregation and their implications on therapeutic strategies, *J. Struct. Biol. 130*, 290−299.
63. Kelly, J. W., Colon, W., Lai, Z., Lashuel, H. A., McCulloch, J., McCutchen, S. L., Miroy, G. J., and Peterson, S. A. (1997) Transthyretin quaternary and tertiary structural changes facilitate misassembly into amyloid, *Adv. Protein Chem. 50*, 161−181.
64. Khare, S. D., Caplow, M., and Dokholyan, N. V. (2004) The rate and equilibrium constants for a multistep reaction sequence for the aggregation of superoxide dismutase in amyotrophic lateral sclerosis, *Proc. Natl. Acad. Sci. U.S.A. 101*, 15094−15099.
65. Cohen, F. E., and Kelly, J. W. (2003) Therapeutic approaches to protein-misfolding diseases, *Nature 426*, 905−909.
66. Ray, S. S., Nowak, R. J., Brown, R. H., Jr., and Lansbury, P. T., Jr. (2005) Small-molecule-mediated stabilization of familial amyotrophic lateral sclerosis-linked superoxide dismutase mutants against unfolding and aggregation, *Proc. Natl. Acad. Sci. U.S.A. 102*, 3639−3644.
67. Taylor, J. R. (1982) *An Introduction to Error Analysis*, University Science Books, Mill Valley, CA.

BI0600953